Quasiparticle excitations in the photoemission spectrum of CuO from first principles: A *GW* study

Claudia Rödl, Francesco Sottile, and Lucia Reining
Laboratoire des Solides Irradiés, École Polytechnique, CNRS, CEA-DSM, 91128 Palaiseau cedex, France
and European Theoretical Spectroscopy Facility (ETSF)

(Received 5 October 2014; revised manuscript received 4 December 2014; published 5 January 2015)

We present *ab initio* quasiparticle calculations for electronic excitations and the fundamental band gap of the strongly correlated transition-metal oxide CuO using the *GW* approximation of many-body perturbation theory. Problems related to the suitability of the method for strongly correlated materials and issues of self-consistency are addressed. We explain why quasiparticle self-consistent *GW* strongly overestimates the band gap of CuO. Apart from the band gap, electron addition and removal spectra in the quasiparticle approximation including lifetime and matrix-element effects are found to be in excellent agreement with the quasiparticle excitations in direct and inverse photoemission data.

DOI: 10.1103/PhysRevB.91.045102 PACS number(s): 71.15.−m, 71.27.+a, 71.45.Gm, 79.60.−i

I. INTRODUCTION

Cupric oxide (CuO), also known as tenorite, features a vast range of applications: it has been used as a pigment in glass and ceramics [1] for thousands of years and is nowadays discussed as a potential absorber material in photovoltaic devices [2] due to its room-temperature band gap of ∼1.4 eV [3,4]. Furthermore, CuO constitutes the building block and parent compound of the cuprate high-temperature superconductors [5]. It is assumed [6] that superconductivity in the cuprates is due to electron-correlation effects in the CuO_2 layers where the Cu ions exhibit the same square-planar coordination with O as it occurs in CuO. Recently, the possibility of high-temperature multiferroicity in CuO has been brought up [7]. All these applications are closely linked to specific properties of the electronic structure. However, surprisingly little is known about the electronic excitations in CuO from a theoretical point of view. This might be due to the fact that the band gap and all electronic excitations in its vicinity are governed by an intricate interplay between itinerant O $2p$ and localized Cu $3d$ electrons which renders the theoretical description notoriously difficult.

CuO crystallizes in a monoclinic face-centered structure (space group: $C2/c$) with four atoms per unit cell [8]. The near degeneracy of several competing equilibrium states in this material is illustrated by the existence of two antiferromagnetic orderings with different Néel temperatures T_N [9,10]. Below $T_N^{(1)} = 213$ K, CuO exhibits the magnetic ordering that is shown in Fig. 1(a) with local magnetic moments in the range of $0.65 \ldots 0.69 \mu_B$ at the Cu atoms [9,10]. In this magnetic structure, each O atom is surrounded by a slightly distorted tetrahedron of four Cu atoms. Three of the surrounding Cu atoms have parallel local magnetic moments, whereas the local moment of the fourth Cu atom points in the opposite direction [9]. Between 213 K and $T_N^{(2)} = 231$ K, the magnetic ordering exhibits a helical structure [10], before the system finally becomes paramagnetic at higher temperatures.

First-principles calculations of the electronic ground state using the non-spin-polarized local-density approximation (LDA) of density-functional theory (DFT) predict CuO to be metallic [11], whereas the experimental direct band gap extrapolated to zero temperature amounts to 1.67 eV [12]. Also spin-polarized LDA calculations do not yield a nonvanishing band gap [13]. Attempts have been made to correct one of the major deficiencies of the LDA, the self-interaction, by removing the corresponding term from the energy functional [13–15]. Even though an insulating ground state can be obtained in this way, the resulting densities of states (DOS) are in qualitative and quantitative contradiction to photoemission data [4,16], since the binding energy of the Cu $3d$ states is seriously overestimated.

Many-body perturbation theory is the method of choice to calculate electron addition and removal spectra from first principles. The *GW* approximation [17,18] to the electronic self-energy has been proven to be successful in the prediction of quasiparticle (QP) band gaps and DOS for semiconductors and other so-called weakly correlated systems [19]. Its applicability to strongly correlated systems, such as transition-metal oxides with open d shells, was contested until a few years ago. However, various groups [20–24] have shown that this "failure" of the *GW* approximation for the magnetically ordered phase of transition-metal oxides is in many cases due to solving the *GW* QP equation in first-order perturbation theory on top of an LDA Kohn-Sham electronic structure. This perturbational approach is applicable to systems with rather delocalized electrons where LDA and QP wave functions can be assumed to be similar [25]. Whenever the spatial distribution of strongly localized orbitals governs the electronic structure—e.g., in transition-metal oxides—nonlocal screened exchange becomes essential and affects also the one-particle wave functions. It can be accounted for by hybrid functionals [26], local exchange-correlation functionals with an additional nonlocal d-d on-site interaction U [27,28], or static approximations to the *GW* self-energy (COHSEX) [17] which may serve as advanced starting points [21–24] for a perturbative solution of the QP equation. Alternatively, the QP equation may be solved self-consistently [20].

Wu *et al.* [29] and Heinemann *et al.* [30] employed hybrid functionals and DFT+U to calculate Kohn-Sham band structures and DOS for CuO. However, these works investigate magnetic orderings different from the magnetic ground state. Rocquefelte *et al.* [31] used a PBE0-derived hybrid functional adjusting the admixture of Fock exchange to recover the experimental values for the local magnetic moments and the band gap. Lany [32] proposed to use an empirical attractive potential for both occupied and unoccupied d states to obtain a *GW* band gap in agreement with experiment.

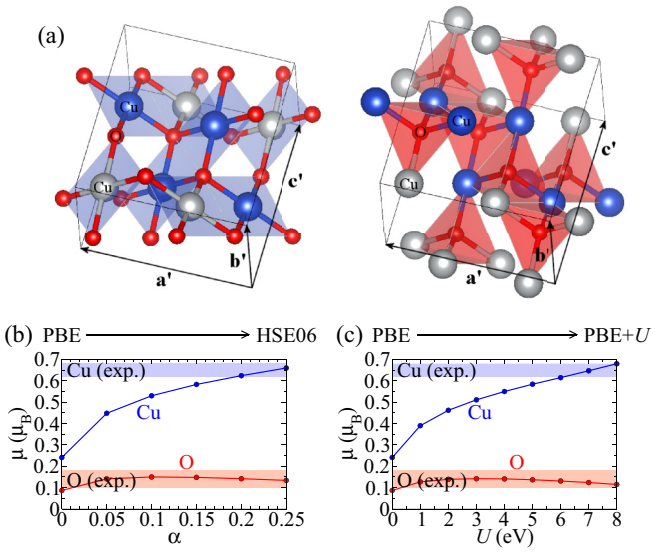

FIG. 1. (Color online) Magnetic ordering and local magnetic moments in CuO. The magnetic unit cell illustrating the ground-state magnetic ordering is displayed in (a). Big white and blue balls represent Cu atoms of opposite spin directions. Small red balls depict O atoms. The approximately square-planar coordination of the Cu atoms (left panel) and the tetrahedral coordination of the O atoms (right panel) are highlighted. The figures have been produced with VESTA [33]. The local magnetic moments μ that occur both at the Cu and O atoms are shown in dependence on the fraction of screened exchange α in the hybrid functional (b) or as a function of the on-site interaction U in the PBE+U approach (c). Experimental values [9] including their error bars are displayed as shaded areas.

Here, we aim to understand the QP excitations in the electron addition and removal spectrum of CuO from first principles. We calculate the band gap and the QP DOS within the GW approximation. The performance of various (partially) self-consistent GW iteration schemes is critically evaluated for this strongly correlated oxide. We find the band gap to be extremely sensitive to the chosen level of approximation. In particular, the dielectric screening employed in the respective GW iteration scheme has a strong impact on the QP gap. The most sophisticated self-consistent solution of the QP equation leads to a huge band-gap overestimation in the case of CuO. Hence, the momentum- and frequency-dependent dielectric function emerges to be a key quantity for describing and understanding the electron addition and removal properties of CuO. Furthermore, we calculate the QP DOS including lifetime and matrix-element effects and compare to direct and inverse photoemission data.

The paper is organized as follows. In Sec. II, the computational details and convergence parameters are summarized. The ground-state properties of CuO and electronic excitations in a DFT framework are briefly discussed in Sec. III. Section IV focuses on a detailed comparison of established GW self-consistency schemes. The band-gap problem and the influence of the electronic screening in the GW self-consistency cycle are addressed. In Sec. V, the resulting QP spectra are compared to experimental photoemission data. Finally, a summary is given and conclusions are drawn in Sec. VI.

II. COMPUTATIONAL DETAILS

Since structural and electronic degrees of freedom are closely entangled in CuO, experimental lattice parameters [8] are used throughout all calculations to avoid spurious effects that may result from deviations between experimental and calculated crystal structures. The experimentally observed antiferromagnetic ordering [9] is described within an eight-formula-unit cell whose lattice vectors are related by $\mathbf{a}' = \mathbf{a} + \mathbf{c}$, $\mathbf{b}' = \mathbf{b}$, and $\mathbf{c}' = -\mathbf{a} + \mathbf{c}$ to the lattice vectors of the conventional face-centered monoclinic chemical unit cell of CuO [see Fig. 1(a)].

DFT and GW calculations are performed using VASP [34–37] with the projector-augmented wave method and a plane-wave cutoff of 450 eV. The Cu 4s, Cu 3d, O 2s, and O 2p electrons are considered as valence states. The Brillouin zone (BZ) is sampled with $3 \times 6 \times 3$ Γ-centered $\mathbf{k}$ points. In the hybrid-functional calculations, the HSE06 functional [26,38] with an inverse screening length $\mu = 0.2$ Å^{-1} and a fraction $\alpha = 1/4$ of short-range Fock exchange is used unless otherwise stated. For the DFT+U calculations, we apply the rotationally invariant scheme [28] on top of the PBE exchange-correlation functional [39]. The choice of the value of U is discussed below. The dielectric screening has been calculated for several functionals using VASP and DP [40].

The HSE06 and PBE+U electronic structures serve as starting points for QP calculations in various well-established GW schemes [20,25,37,41]. In all GW calculations, the screening is evaluated at 200 frequency points taking into account plane waves up to a cutoff of 200 eV. Both in the computation of the correlation self-energy and the electronic screening, 384 bands [corresponding to energies up to ∼80 eV above the valence-band maximum (VBM)] are included. To reduce the computational workload and render self-consistent calculations feasible, the BZ sampling is reduced to a mesh of $2 \times 3 \times 2$ $\mathbf{k}$ points in the self-consistent GW calculations which does not have a significant impact on the band gap or the DOS.

Recently, concerns have been raised about the notoriously slow convergence of GW band gaps with the number of empty bands in the self-energy and the plane-wave cutoff in the screening function, especially when the orbital characters of the lowest conduction band and the highest valence band are distinct, e.g., s and p states [43–45]. Even though in CuO the influence should be minor, since both VBM and conduction-band minimum (CBM) feature mixed pd character, the robustness of our results has been tested in this respect. We performed perturbative G_0W_0 calculations with norm-conserving PAW pseudopotentials [46] including only the Γ point but up to 6144 bands (∼640 eV above the VBM) and plane waves up to a cutoff of 500 eV in the screening matrix. The results indicate that the GW band gaps of CuO are converged for the set of parameters specified earlier. Indeed, we observe that both the VBM and CBM shift slowly to lower energies when the numbers of bands is increased for a fixed high cutoff in the screening matrix. Including more plane waves allows for a more accurate description of the localized states as well as their overlap with plane-wave-like high-lying conduction states in the screening matrix. The improved description of the correlation self-energy leads to a lowering in energy of the d-like states in the valence and low conduction

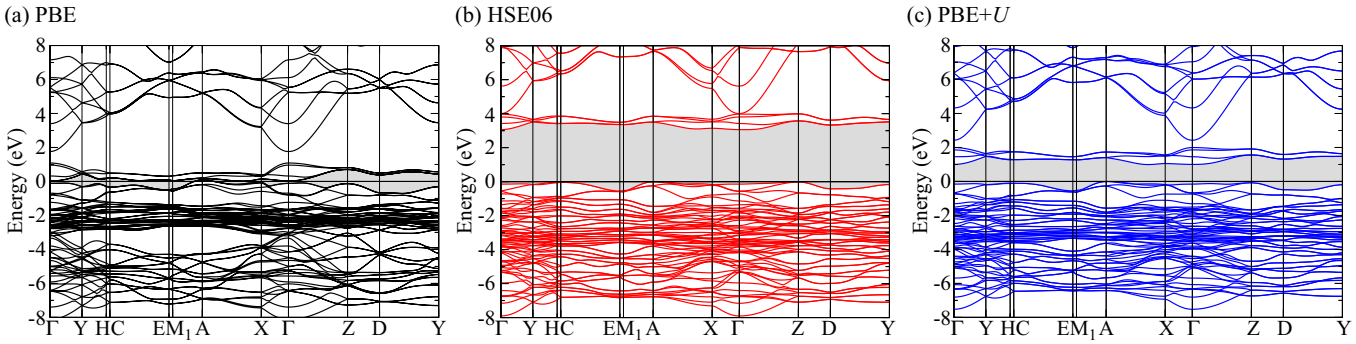

FIG. 2. (Color online) Kohn-Sham band structures calculated with the PBE (a), HSE06 (b), and PBE+U ($U = 4$ eV) (c) functionals. The VBM is set to zero and the band gap is highlighted as shaded area. The nomenclature of the high-symmetry points follows Ref. [42].

bands [43,46]. However, in CuO, the difference between the CBM and the VBM, i.e., the band gap, converges much faster thanks to error cancellations that are due to the identical orbital character (see Sec. III A) of the gap-forming states.

III. GROUND STATE AND ELECTRONIC EXCITATIONS WITHIN DFT

Before discussing the excitation spectra, we briefly characterize the ground-state properties of CuO to illustrate the mechanisms that lead to an insulating ground state with magnetic moments as found in experiment.

A. Band structures and DOS

In Fig. 2, the DFT Kohn-Sham band structures of CuO calculated with the PBE, HSE06, and PBE+U (with $U = 4$ eV) functionals are displayed. As has been shown before [11,29], (semi)local density functionals yield a metallic ground state with a closely entangled band complex of O $2p$ and Cu $3d$ states around the Fermi energy [see Fig. 2(a)]. In particular, the highest valence band in the vicinity of the A point of the BZ is unoccupied, i.e., it exhibits a hole pocket. Contrary to the metallic PBE band structure, the HSE06 and PBE+U band structures feature indirect band gaps of 3.1 and 1.1 eV, respectively (see Table I). It is worthwhile to investigate the mechanism of gap formation in more detail.

TABLE I. Indirect (ind.) and direct (dir.) QP band gaps calculated in various flavors of the GW approximation starting from HSE06 and PBE+U ($U = 4$ eV) electronic structures. Furthermore, the band gaps obtained in the self-consistent COHSEX approximation are given. In all cases, the fundamental gap is indirect. If indirect and direct gap happen to have the same value, this is due to rounding on one decimal place.

Gap (eV)		DFT	G_0W_0	G_nW_0	G_nW_n	scG_nW_0	scG_nW_n
HSE06	ind.	3.1	3.5	3.7	3.8	3.7	4.1
	dir.	3.2	3.6	3.8	3.9	3.8	4.2
PBE+U	ind.	1.1	1.7	1.9	2.2	2.2	3.9
	dir.	1.2	1.8	2.0	2.3	2.2	4.1
COHSEX	ind.						4.0
	dir.						4.0

The band gap in DFT is given by the Kohn-Sham band gap and the discontinuity of the exchange-correlation potential upon electron addition and removal [47,48]. Generalized Kohn-Sham functionals that include nonlocal exchange account for a good fraction of the discontinuity already in the generalized Kohn-Sham band gap [49]. The failure of LDA and related functionals to open a gap can be partially traced back to the complete absence of the discontinuity in the exchange-correlation potential. Several orbital-dependent functionals have been proposed to improve the eigenvalue band gaps upon (semi)local Kohn-Sham functionals [49–51]: (i) hybrid functionals with a fraction α of (short-range) exchange, where the inverse of α can be related to the static electronic dielectric constant; (ii) self-interaction-corrected density functionals; (iii) density functionals with an additional on-site interaction U which is inspired by the multiband Hubbard model. In principle, U represents the screened on-site interaction in a solid which can be much smaller than the corresponding atomic value. Even though several schemes for the determination of U exist [51,52], it is often chosen such that it reproduces the experimental value of a specific property of the electronic structure (e.g., the band gap).

In Fig. 3(a), the evolution of the orbital-resolved DOS with increasing fractions of short-range screened exchange α in the HSE hybrid exchange-correlation functional is shown. The parameter α is varied between 0 (PBE) and 0.25 (HSE06). It becomes immediately clear from Fig. 3(a) that the Cu $3d_{xy}$, $3d_{yz}$, $3d_{zx}$, and $3d_{z^2}$ states do not take part in the band-gap formation. These orbitals, which are more or less degenerate in energy and hybridize only weakly with the O $2p$ states, are occupied for both spin directions and lie, rather independent of the value of α, in the energy range between 2 and 4 eV below the VBM. The Cu $3d_{x^2-y^2}$ states, on the other hand, strongly hybridize with the O $2p$ states. In the PBE approach, they form one band complex 4 to 8 eV below the VBM and a second one around the Fermi level. Increasing the fraction of Fock exchange leads to an imbalance between the spin-up and spin-down channels which goes along with the formation of a magnetic moment at the Cu atoms (see below). While the $d_{x^2-y^2}$ orbital becomes unoccupied for one spin direction, thus forming the CBM, the $d_{x^2-y^2}$ state in the opposite spin direction contributes, due to its hybridization with the O $2p$ states, to the bottom as well as the top valence states. The details of the crystal structure and the size of the band gap are intimately linked via this hybridization.

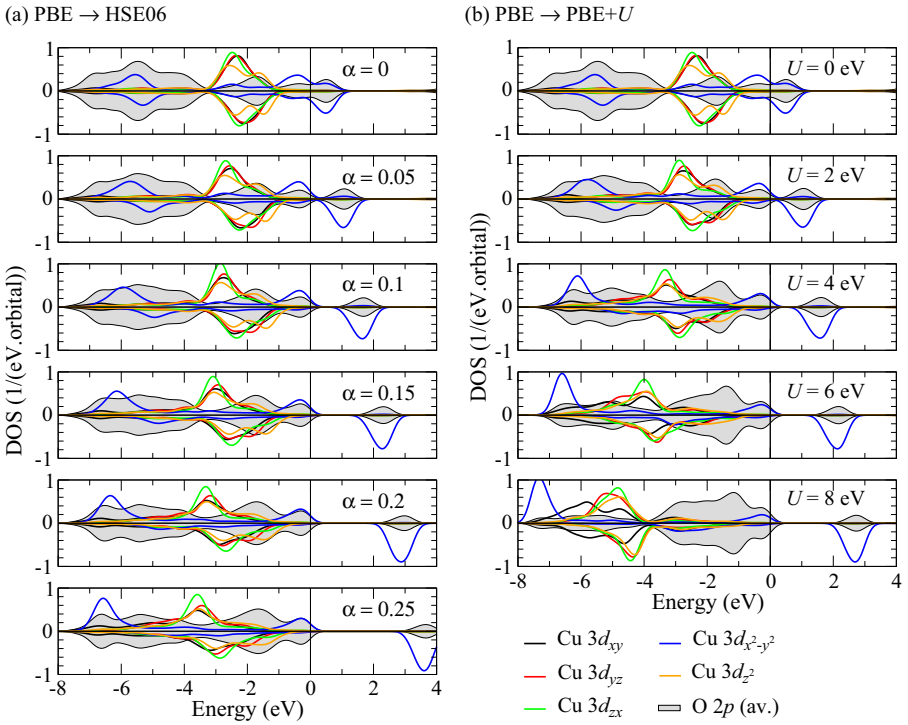

FIG. 3. (Color online) Orbital-projected DOS calculated with the hybrid functional for varying α (a) or with the PBE+U functional for varying U (b). The spin-up (positive values) and spin-down (negative values) contributions of the individual Cu $3d$ orbitals and the O $2p$ orbitals are shown. The local coordinate system at the Cu atoms is oriented such that the z axis is perpendicular to the Cu-O coordination square and the x axis parallel to a Cu-O bond. For the O $2p$ partial DOS, the average contribution per O atom is shown. The VBM is set to zero and all DOS are convoluted with a Gaussian of 0.5 eV full width at half maximum (FWHM).

If, instead of a fraction of short-range Fock exchange, one adds a d-d on-site interaction U to the PBE exchange-correlation functional [see Fig. 3(b)], a very similar behavior of the electronic states is observed for small $U \lesssim 4$ eV. Also in this case, the minority-spin $d_{x^2-y^2}$ state becomes unoccupied, while the majority-spin $d_{x^2-y^2}$ orbital hybridizes with the O $2p$ states. If, however, the on-site term is increased further, the occupied $d_{x^2-y^2}$ orbital moves to the bottom valence, whereas the O $2p$ orbitals form the top-valence states. Since the on-site interaction acts on all $3d$ orbitals, also the inert Cu $3d_{xy}$, $3d_{yz}$, $3d_{zx}$, and $3d_{z^2}$ states shift to lower energies which does not happen if a hybrid functional is employed.

The band gap is sensitive to the details of the antiferromagnetic ordering. Several previous studies [29,30] did not investigate the experimentally observed ground-state magnetic ordering but other antiferromagnetic structures. Consequently, they find band gaps that are significantly lower. For instance, in Ref. [30], an indirect HSE06 band gap of 2.7 eV has been reported. Reproducing the HSE06 calculation with the magnetic ordering used in Ref. [30], we obtain an indirect gap of 2.5 eV significantly lower than the 3.1 eV we find for the ground-state magnetic ordering.

B. Magnetic moments

The calculated magnetic moments at the Cu and O atoms are shown in Figs. 1(b) and 1(c) in comparison to data from neutron-diffraction experiments [9]. The screening parameter α and the on-site interaction U have been varied in these plots to illustrate their influence on the value of the local magnetic moment. Best agreement with experiment is obtained for $\alpha = 0.25$ and $U \sim 7$ eV. However, modelling the complex many-body interaction by tuning a single scalar parameter cannot capture all effects of the electronic self-energy. The optimal choice of the respective parameter depends on the quantity that is calculated. In particular, it may be different for ground-state (lattice constants, magnetic moments) and excited-state properties (band structures, densities of states). For instance, the frequency dependence of the U parameter has been illustrated by mapping the full dynamical screened Coulomb interaction to local orbitals [52]. For reasons explained in Sec. IV B, we will later on choose the electronic structure computed with $U = 4$ eV as one of the starting points for the calculation of excitation properties. Here, we give results for both values $U = 4$ eV and $U = 7$ eV.

A peculiarity of CuO is the occurrence of a local magnetic moment not only at the transition-metal atoms, but also at the O atoms which is a consequence of the interplay between the complex magnetic ordering and the crystal structure: each O atom is embedded in a tetrahedral environment of four Cu atoms whereof one exhibits a magnetic moment pointing in the direction opposite to the magnetic moments of the three other Cu atoms [see Fig. 1(a)], which leads to a magnetic polarization of the electrons in the vicinity of the O atom. At the O atoms, we find local magnetic moments of $0.13\mu_B$ (HSE06), $0.14\mu_B$ (PBE+U, $U = 4$ eV), and $0.12\mu_B$ (PBE+U, $U = 7$ eV) that are in line with experiment ($0.14 \pm 0.04\mu_B$, Ref. [9]) and previous calculations [15,31]. The Cu magnetic moment amounts to $0.66\mu_B$ (HSE06), $0.55\mu_B$ (PBE+U, $U = 4$ eV), and $0.65\mu_B$ (PBE+U, $U = 7$ eV), which agrees well with experimental values of $0.65 \pm 0.03\mu_B$ [9] and $0.69 \pm 0.05\mu_B$ [10].

IV. ELECTRONIC EXCITATIONS WITHIN THE *GW* APPROACH

Band gaps calculated from Kohn-Sham electronic structures are not directly comparable to experimental gaps. The Kohn-Sham gap differs from the QP gap by the contribution arising from the derivative discontinuity of the

exchange-correlation energy which accounts for electron addition and removal [47,48]. Generalized Kohn-Sham functionals, such as the HSE06 hybrid functional, take this term partially into account already in the eigenvalue gap [49] but are still suffering from the fact that the exact exchange-correlation potential is unknown. Green's function methods, such as the GW approach, on the other hand, include the electron addition and removal aspect by construction.

The GW self-energy $\Sigma_{GW}(12) = i\hbar G(12)W(12)$ is the product of the one-particle Green's function $G(12)$ and the screened Coulomb interaction $W(12) = \int d3\varepsilon^{-1}(13)v(3-2)$, with the inverse dielectric function $\varepsilon^{-1}(12)$ and the bare Coulomb interaction $v(1-2) = \frac{1}{4\pi\varepsilon_0}\frac{e^2}{|\mathbf{r}_1-\mathbf{r}_2|}\delta(t_1-t_2)$. In these expressions, numbers are used as shorthand for the set of space, spin, and time coordinates, i.e., $1 \equiv \mathbf{r}_1, s_1, t_1$. Usually, the screened interaction is calculated in the random-phase approximation (RPA), i.e., neglecting the electron-hole interaction [17,18].

QP states $|\psi_i\rangle$ can be obtained by solving the QP equation [18]

$$[T + V + V_{\mathrm{H}} + \Sigma_{GW}(\varepsilon_i)]|\psi_i\rangle = \varepsilon_i|\psi_i\rangle \tag{1}$$

self-consistently. Here, T denotes the kinetic energy, V the external potential, V_{H} the Hartree potential of the electrons, and $\Sigma_{GW}(\omega)$ the GW self-energy in frequency space, which has to be taken at the energy of the QP excitation ε_i. Usually, the QP equation is solved starting from Kohn-Sham eigenvalues $\varepsilon_i^{(0)}$ and wave functions $|\varphi_i\rangle$ either in first-order perturbation theory or applying (partially) self-consistent iteration schemes.

Assuming that Kohn-Sham wave functions $|\varphi_i\rangle$ and QP wave functions $|\psi_i\rangle$ are identical and, hence, that both the QP Green's function and the difference between self-energy and exchange-correlation potential are approximately diagonal in these wave functions, the QP equation reduces to

$$\varepsilon_i = \mathrm{Re}\langle\varphi_i|[T + V + V_{\mathrm{H}} + \Sigma_{GW}(\varepsilon_i)]|\varphi_i\rangle. \tag{2}$$

Keeping the wave functions fixed and iterating only over the eigenvalues [25,37], the QP energies in the $(n+1)$th iteration step are then given by

$$\varepsilon_i^{(n+1)} = \varepsilon_i^{(n)} + Z_i^{(n)} \times \left(\mathrm{Re}\langle\varphi_i|\left[T + V + V_{\mathrm{H}} + \Sigma_{GW}^{(n)}\left(\varepsilon_i^{(n)}\right)\right]|\varphi_i\rangle - \varepsilon_i^{(n)}\right), \tag{3}$$

with the QP renormalization factor

$$Z_i^{(n)} = \left(1 - \frac{\partial\ \mathrm{Re}\langle\varphi_i|\Sigma_{GW}^{(n)}(\omega)|\varphi_i\rangle}{\partial\omega}\bigg|_{\hbar\omega=\varepsilon_i^{(n)}}\right)^{-1}. \tag{4}$$

In this expression, the self-energy has been linearized around the QP pole. The matrix elements of the GW self-energy $\langle\varphi_i|\Sigma_{GW}^{(n)}(\omega)|\varphi_i\rangle$ are recalculated in each step using the Kohn-Sham wave functions and the QP eigenvalues obtained in the previous iteration. Depending on whether the energy eigenvalues that enter Σ_{GW} are updated in G only or both in G and W, the iteration scheme is called G_nW_0 or G_nW_n, respectively. In the simplest approach, only one iteration is performed and the energy eigenvalues are corrected in first-order perturbation theory (G_0W_0).

Alternatively, one can try to solve Eq. (1) directly which allows one to obtain also QP wave functions. However, the frequency-dependent self-energy operator $\Sigma_{GW}(\omega)$ renders this equation non-Hermitian and nonlinear which results in QP excitations with finite lifetime and renormalized intensity. Several procedures known as QP self-consistent GW have been proposed to construct an eigenvalue problem with a Hermitian Hamiltonian from Eq. (1) [20,41,53,54]. The resulting QP eigenvalues differ only marginally between these procedures [41]. In all of these GW schemes, the Green's function retains its noninteracting form and lifetime effects are neglected. Here, we follow the approach presented in Ref. [41]. We refer to it as scG_nW_0 or scG_nW_n depending on whether G only or both G and W are recalculated with the new set of eigenstates in each self-consistency step. The numerical implementation of this scheme yields band gaps in good agreement with experiment for weakly correlated materials. For transition-metal oxides and f-electron systems, however, d-d or f-f gaps are systematically overestimated [20,53,55]. It has been proposed to scale the self-energy with a prefactor of 0.8 in order to mimic the effects of vertex corrections empirically [55]. For instance, the rescaling of the self-energy compensates for the systematically underestimated dielectric constants in the scG_nW_n iteration scheme. Shishkin *et al.* [41] suggested to either include an exchange-correlation kernel in W to account for the excitonic effects or to keep W fixed on the DFT RPA level.

All of these flavors of GW self-consistency have been applied to a large variety of materials in the past. Here, we investigate how the different approaches perform for the DOS and band gap in the case of CuO. We analyze and discuss shortcomings of the methods that are expected to be characteristic for materials similar to CuO.

A. Perturbative G_0W_0

In Sec. III, it has been shown that both hybrid functionals and PBE+U yield insulating electronic structures for CuO. Here, we consider these electronic structures as possible starting points for GW calculations in the perturbative G_0W_0 approach.

In Fig. 4(a), the DOS calculated within the G_0W_0 approximation are shown in comparison to the subjacent hybrid-functional calculation for various values of the screening parameter α. We notice that the general line shape of the DOS barely changes if G_0W_0 corrections are added. This finding holds for the whole range of investigated parameters α. Only the band gap opens significantly—even for values of α where the hybrid functional already overestimates the experimental gap [cf. Fig. 4(c)]. Moreover, the band gap increases linearly with increasing screening parameter α.

On the one hand, this illustrates the strong starting-point dependence of non-self-consistent GW calculations. On the other hand, it yields valuable insight into the mechanisms that govern the band-gap formation in CuO within the GW framework, i.e., a picture of QPs screened by electron-hole excitations. It indicates that the hybrid-functional ansatz already captures most of the many-body effects that govern the energetic ordering of the states but fails in a similar way as the subsequent G_0W_0 calculation to predict the band gap.

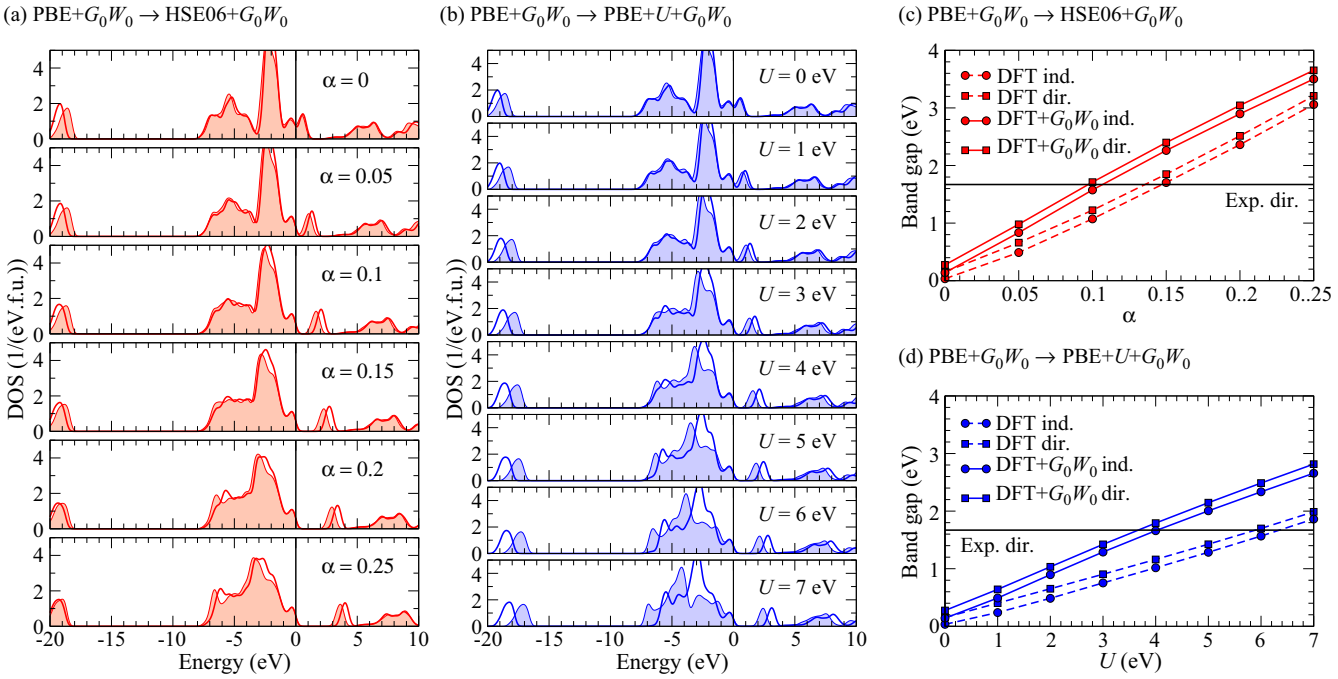

FIG. 4. (Color online) DOS as well as indirect (ind.) and direct (dir.) band gaps calculated in the G_0W_0 one-shot approach on top of the hybrid functional for varying α [(a),(c)] and the PBE+U functional for varying U [(b),(d)]. The respective DFT DOS is shown as shaded area, whereas the G_0W_0 DOS is indicated by a thick solid line. The VBM is set to zero. A Gaussian broadening of 0.5 eV is applied to the DOS. In (c) and (d), the experimental direct band gap at zero temperature [12] (cf. Table II), represented by a black horizontal line, is given for reference.

In particular, there does not seem to be a mechanism in G_0W_0 that compensates a band-gap overestimation in the subjacent hybrid-functional calculation.

Indeed, the HSE hybrid functional can be seen as a static approximation to the GW self-energy with the parameter α as inverse electronic static dielectric constant $1/\varepsilon_\infty$. The range-separation parameter which cuts down the Fock exchange for large distances acts as a screening length. Thus the HSE06 hybrid functional mimics already the important static screened-exchange contribution to the GW self-energy. This explains why setting $\alpha = 1/4$ (HSE06) yields good band gaps for intermediate-gap semiconductors with dielectric constants in the range of $\sim 2 \ldots 6$ (see compilations in Refs. [56–58]) and why it is less accurate for strongly polarizable materials like Si with $\varepsilon_\infty = 11.94$ [59]. For CuO, a band gap of 1.42 eV was obtained by setting $\alpha = 0.15$ in a hybrid functional with infinite screening length (PBE0-derived functional) [31]. For $\alpha = 0.15$ and an inverse screening length of $\mu = 0.2$ Å^{-1}, we obtain an indirect gap of 1.7 eV and a direct gap of 1.9 eV (see Fig. 4). This observation is in line with the interpretation of α as inverse dielectric constant which amounts to $\varepsilon_\infty = 6.2 \ldots 6.6$ in CuO [60–62].

In Fig. 4(b), we choose, instead of a hybrid functional, a PBE+U electronic structure as starting point for the G_0W_0 calculation. We find that, in particular for large values of U, the QP shifts are significantly bigger for some states compared to the QP shifts obtained for the hybrid functional starting point. For instance, the G_0W_0 corrections shift the O 2s states in the vicinity of -19 eV to significantly higher binding energies. G_0W_0 also tries to correct back the energetic position of the occupied Cu 3d states that are shifted to too high binding energies by large values of U in PBE+U. All in all, this indicates that PBE+U, in general, is a less good approximation to the GW self-energy which is intuitively clear, since it mostly affects the d states and does not provide an advanced description of exchange and correlation for the s and p states.

As expected, we find the PBE+U band gaps to increase linearly with U illustrating the d-d character of the highest valence and lowest conduction states [cf. Fig. 4(d)]. However, the G_0W_0 band gap increases with an even higher slope in dependence on U. For large U [e.g., $U = 7$ eV in Fig. 4(d)], where the gap is already overestimated, the band-gap opening due to G_0W_0 QP shifts is largest demonstrating the sensitivity of the results on the input electronic structure.

B. Eigenvalue self-consistent GW

Since self-consistent GW calculations are numerically very demanding, we focus on the comparison between two starting electronic structures from now on: (i) HSE06 ($\alpha = 1/4$) and (ii) PBE+U with $U = 4$ eV. These two starting points feature the peculiarity that their (state-projected) DOS are basically identical (see Fig. 3) except for strongly deviating band gaps which amount to 3.1 eV in the case of HSE06 and 1.1 eV for PBE+U (cf. Table I). In particular, the HSE06 band gap is almost twice as large as the experimental gap (see Table II), which is unusual for a 3d transition-metal monoxide [23,64]. A comparison between these two starting points may thus be helpful to understand the origin of the GW band-gap overestimation in CuO.

As we have seen in Sec. III, the energetic position of the Cu $3d_{x^2-y^2}$ peaks and, in particular, the size of the band gap strongly depend on the choice of the exchange-correlation functional which cannot be cured by G_0W_0 QP corrections.

TABLE II. Available indirect (ind.) and direct (dir.) experimental gap values and their temperature dependence.

Gap (eV)	300 K	7 K	0 K
ind.	1.35 ± 0.02[a] 1.4 ± 0.3[b]		
dir.	1.34[c]	1.60[d]	1.67[e]

[a]Reference [3]; electrochemical determination of the photocurrent in *p*-type CuO.
[b]Reference [4]; x-ray photoemission and bremsstrahlung-isochromat spectroscopy.
[c]Reference [12]; reflectance and transmittance.
[d]Reference [63]; optical absorption, 7 K.
[e]Reference [12]; reflectance and transmittance, extrapolated to 0 K removing zero-point motion.

This underlines the need for a starting-point independent approach. QP calculations that keep the wave functions fixed but iterate the one-particle eigenvalues constitute a first step towards self-consistency.

In Table I, the indirect and direct QP band gaps of CuO are compiled for various self-consistent GW schemes. It is evident that, keeping the wave functions fixed, the band gap changes only very little compared to a G_0W_0 calculation. Convergence of the band gap is obtained after a few iteration steps (see Fig. 5). This holds likewise for the G_nW_0 and the G_nW_n iteration scheme and is independent of the starting point. However, the resulting values for the band gaps are strongly starting-point dependent. The PBE+U+G_nW_0/G_nW_n band gaps overestimate the experimental value only slightly, whereas the HSE06+G_nW_0/G_nW_n gaps are by more than a factor of 2 too large. Hence it can be concluded that wave-function self-consistency is highly important in CuO and, concomitantly, that QP and Kohn-Sham wave functions

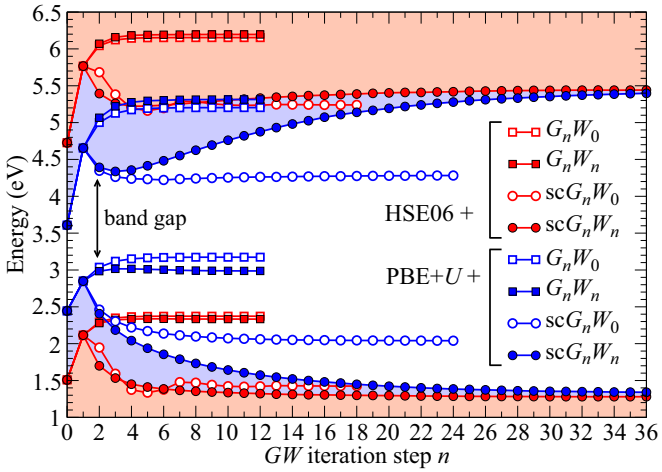

FIG. 5. (Color online) Convergence of the highest valence band and lowest conduction band at Γ with the number of iteration steps n in various flavors of the GW approximation. Results are given for HSE06 and PBE+U starting electronic structures. The zeroth iteration step corresponds to the DFT eigenvalues.

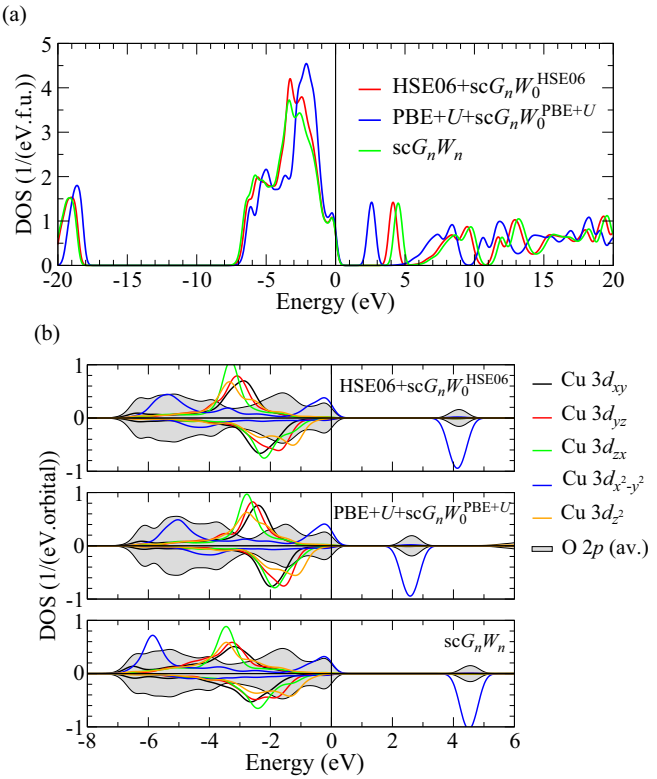

FIG. 6. (Color online) Full (a) and orbital-resolved (b) DOS of CuO for various self-consistent GW schemes. The screened Coulomb interaction W is either fixed (W_0) to the subjacent DFT starting point (HSE06 and PBE+U) or iterated to self-consistency (W_n). In the latter case, the resulting DOS is independent of the starting point. The DOS are broadened with a Gaussian of 0.5 eV (FWHM) and the VBM is set to zero.

differ significantly in this material for the chosen generalized Kohn-Sham schemes.

C. Quasiparticle self-consistent GW

A self-consistent solution of the Hermitianized and linearized QP equation (1) should be essentially independent of the starting electronic structure. Indeed, we find that applying the scG_nW_n scheme to both starting points the electronic QP structures converge—even though slowly—to the same solution. This is illustrated for the VBM, the CBM, and, hence, the band gap in Fig. 5. The remaining deviations in the scG_nW_n gaps for the two starting points in Table I are due to the finite number of iteration steps. In Fig. 6, the resulting DOS as well as the orbital-projected DOS are plotted only once, since the curves for the two starting points are indistinguishable. We do not find the starting-point dependence that Liao *et al.* [65] observed for Fe_2O_3. However, we want to emphasize that convergence is hard to achieve and that in self-consistency cycles errors may accumulate.

Despite the line shape of the DOS being still very similar to the DFT results, the resulting band gap of more than 4 eV overestimates the experimental value by a factor of 2.5 (see Tables I and II). Even though a slight band-gap overestimation seems to be inherent to this approach, the discrepancy between scG_nW_n band gap and experimental band gap is striking for CuO.

D. Influence of the screening

The dramatic gap overestimation for CuO within the scG_nW_n scheme asks for a more detailed understanding. Let us assume for the moment that $\Sigma(12) = i\hbar G(12)W(12)$ is a good approximation for the full self-energy which reads $\Sigma(12) = -i\hbar \int d(34)G(13)W(14)\Gamma(324)$, with Γ being the vertex function that describes, for instance, electron-hole interactions in the screening or particle-particle interactions in the self-energy [18]. This means that, in the GW approximation, vertex corrections in the self-energy and thus contributions that are of second or higher order in the screened interaction (e.g., T-matrix diagrams) are neglected. However, the vertex function occurs also in the dielectric function $\varepsilon(12) = \delta(1-2) - i\hbar \int d(345)v(1-3)G(35)G(43)\Gamma(542)$ whose inverse governs the dynamically screened Coulomb interaction.

In the original formulation of Hedin's equations [17,18], the dielectric screening that enters the GW self-energy has to be evaluated in RPA, $\varepsilon(12) = \delta(1-2) + i\hbar \int d3v(1-3)G(32)G(23)$. Indeed, it has been shown that a screened Coulomb interaction calculated in RPA with independent-particle Green's functions constructed from a Kohn-Sham electronic structure yields results that are in good agreement with experiment for many semiconductors (see, e.g., Ref. [19]). This is due to an error cancellation between the neglected QP corrections in the Green's functions and the omission of the electron-hole attraction, i.e., excitonic effects.

The scG_nW_n scheme, on the other hand, updates wave functions and eigenvalues in W which corresponds to an inclusion of QP shifts, whereas the electron-hole interaction is still omitted. This leads to a systematic underestimation of the dielectric screening and, consequently, to too high band gaps [41]. The same effect can be observed already in the self-consistent static COHSEX (Coulomb hole plus screened exchange) approximation [17] to the GW self-energy. Even neglecting completely the frequency dependence of the screening throughout the self-consistency cycle, the strong band-gap overestimation can be reproduced. Self-consistent COHSEX yields a gap of 4.0 eV comparable to the scG_nW_n gap (cf. Table I).

In Fig. 7, the evolution of the macroscopic electronic static dielectric constant ε_∞ of CuO with the number of iteration steps in the G_nW_n and scG_nW_n schemes is shown. The respective values of ε_∞ for the iteration schemes where W is not subject to changes (G_nW_0 and scG_nW_0) correspond to the zeroth iteration. The dielectric constant of 10.3 in PBE+U+G_0W_0 (iteration step $n = 0$) is by far higher than the experimental values of 6.45 [61], 6.2 [60], and 6.6 [62]. The G_nW_n iteration scheme reduces ε_∞ to 7.6, whereas it decreases even well below the experimental value in the scG_nW_n approach. For the HSE06 starting point, on the other hand, changes are minor, since already in the G_0W_0 step $\varepsilon_\infty = 4.7$, which is further reduced to 4.5 (G_nW_n) or 4.1 (scG_nW_n). These values underestimate the experimental screening constant which is in line with the observed band-gap overestimation.

Little is known about the wave-vector and frequency dependence of the dielectric screening from experiment. Recently, the low-energy d-d excitations have been measured for high momentum transfers [66,67]. The only available data

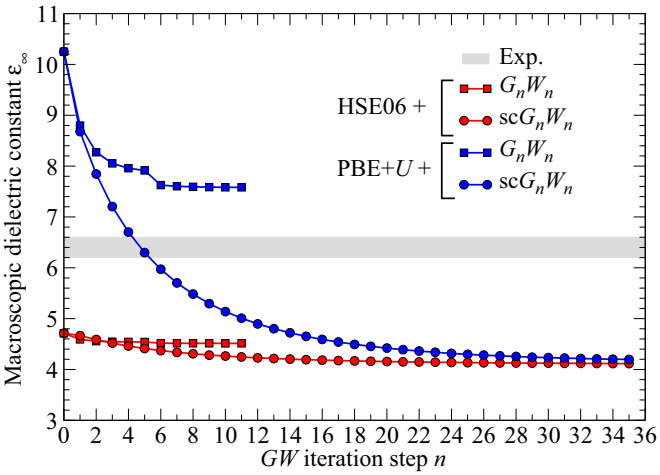

FIG. 7. (Color online) Convergence of the macroscopic electronic static dielectric constant ε_∞ (averaged over directions) with the number of iteration steps n in various flavors of the GW approximation. Results are given for HSE06 and PBE+U starting electronic structures. The zeroth iteration step corresponds to the macroscopic dielectric constant ε_∞ deduced from W_0. The range of available experimental values as the high-frequency limit of infrared [60,62] and the low-frequency limit of optical [61] spectroscopy is given as shaded area.

in a wide frequency range is the loss function $-\mathrm{Im}\,\varepsilon^{-1}(\mathbf{q},\omega)$ for vanishing momentum transfer $\mathbf{q} = 0$ (see Fig. 8). In Fig. 8, loss functions calculated in the RPA with the HSE06, PBE+U, and scG_nW_n electronic structures are compared to momentum-integrated electron-energy loss spectra [68] and inverted spectroscopic ellipsometry data [61]. In the literature, loss functions are most often calculated from electronic

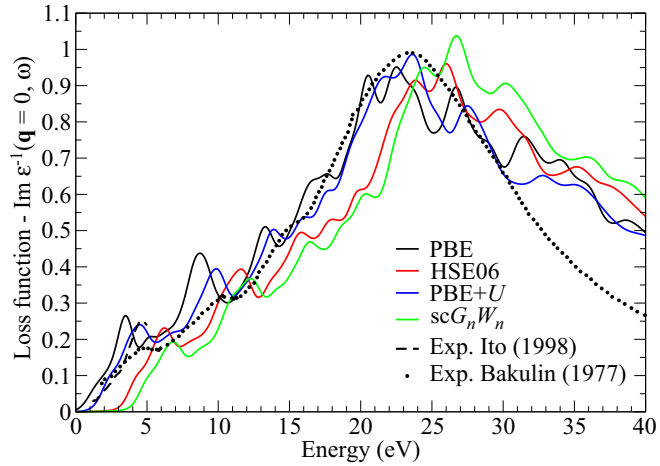

FIG. 8. (Color online) Frequency-dependent loss function of CuO for vanishing momentum transfer $\mathbf{q} = 0$ averaged over Cartesian directions. The loss function $-\mathrm{Im}\,\varepsilon^{-1}(\mathbf{q} = 0,\omega)$ is calculated in RPA using the DFT electronic structures of the two GW starting points (HSE06 and PBE+U) and the self-consistent scG_nW_n QP electronic structure. The direction-averaged loss function is compared to experimental data from spectroscopic ellipsometry [61] and electron-energy loss [68]. For completeness, the loss function calculated in RPA using the metallic PBE electronic structure is also given.

structures that have been obtained with a (semi)local density functional. For this reason, we provide also the loss function computed from PBE wave functions and eigenvalues for comparison, keeping in mind that PBE predicts CuO to be a metal.

The experimental loss data shown in Fig. 8 exhibit a broad plasmon peak around 23 eV and some fine structure at lower energies. The PBE, HSE06, PBE+U, and scG_nW_n calculations all recover the general line shape of the experimental loss spectrum; only the absolute peak positions are subject to a rigid energy shift that depends on the band gap of the respective electronic structure. The discrepancies between measured and calculated spectra at energies above the main plasmon are attributed to the $\mathbf{q}$ integration in the experimental loss spectrum which is due to its limited momentum resolution (cf., e.g., Ref. [69]). Both the main plasmon peak and the fine structure in the loss spectrum at low energies, in particular the pronounced peaks near 5 and 10 eV, are best described within the PBE+U approach.

E. Self-consistent GW with fixed screening

1. Fixed RPA electronic screening

The GW formalism links the dielectric screening, that is experimentally accessible through loss experiments, to quantities like the photoemission band gap or the QP DOS. Here, we investigate how changes in the screening affect the QP energies and the band gap. In the previous section, it has been shown that the PBE+U RPA screening compares excellently to experiment for small $\mathbf{q}$, i.e., in the long range which is usually dominant in the GW approach. In this spirit, we start from the PBE+U electronic structure and solve the QP equation (1) self-consistently without changing the matrix elements of W throughout the iteration (PBE+U+sc$G_nW_0^{\mathrm{PBE}+U}$). For the purpose of comparison, the same procedure is carried out for the HSE06 starting point.

The resulting band gaps can be found in Table I and Fig. 5. Of course, the result cannot be starting-point independent anymore. Using the HSE06 screening, we obtain an indirect band gap of 3.7 eV only marginally smaller than in the scG_nW_n approach. This is not unexpected considering the blueshift of all loss peaks in the HSE06 dielectric function (see Fig. 8). If, however, the PBE+U screening—which agrees much better with experiment for the available $\mathbf{q}=0$ spectrum (cf. Fig. 8)—is used, we find a band gap of 2.2 eV which is already much closer to experiment, though still a little too high.

2. Estimate of polaronic screening contributions

The remaining difference between experimental and theoretical band gap might well be due to details of the screening, but it also raises the question whether other physical effects such as polarons contribute to the discrepancy. Taking into account polaronic excitations affects the band gap in two ways. (i) At nonzero temperatures, phonon states above the ground state will be occupied resulting in smaller band gaps. Thus the calculated band gaps have to be compared to experimental gaps at 0 K. (ii) Polarons may be excited during the photoemission experiment (even at zero temperature) and contribute to the screening of the Coulomb interaction which leads to a band-gap shrinkage.

In Table II, we compare the available experimental gap values for different temperatures. High-resolution optical data have been measured between 10 and 300 K and extrapolated to 0 K removing also the zero-point motion [12]. The resulting direct gap is found to be 1.67 eV at 0 K. An absorption study [63] conducted at 7 K reported the direct gap to be 1.60 eV (including zero-point motion) which is consistent with the other experiment. The indirect band gap, however, has been measured only at room temperature and was found to be 1.35 ± 0.02 eV [3] or 1.4 ± 0.3 eV [4]. Assuming that the gap-forming bands are essentially flat due to their d character, this is consistent with the room-temperature direct gap of 1.34 eV reported in Ref. [12].

Botti *et al.* [70] have shown recently that polaronic screening may reduce GW band gaps by about 15% in strongly polarizable materials like MgO. However, it is unlikely that polaronic screening can explain our results. The biggest gap renormalization due to polaronic screening is expected for materials with a small electronic static screening constant ε_∞ and a big static screening constant ε_0 [since the polaron coupling constant is proportional to $(1/\varepsilon_\infty - 1/\varepsilon_0)$] as well as large longitudinal optical phonon frequencies ω_{LO} [71,72]. For instance, in MgO, the dielectric constants amount to $\varepsilon_\infty = 2.94$ and $\varepsilon_0 = 9.83$, while ω_{LO} is 89 meV [73].

In CuO, the electronic static dielectric constant amounts to $\varepsilon_\infty = 6.6$ (averaged over directions, Ref. [62]), whereas the static dielectric screening constant including lattice polarizability is $\varepsilon_0 = 11.1$ (averaged over directions, derived from the fit parameters given in Ref. [62]). The longitudinal optical phonon frequencies lie in the energy range between 19 and 78 meV [62]. From these values, one can expect polaronic screening contributions in CuO to be lower than in MgO. Taking into account these considerations, the overestimation of the experimental band gap of 2.2 eV by about 30 % in the PBE+U+sc$G_nW_0^{\mathrm{PBE}+U}$ approach seems to be too large to be explained solely by polaronic effects.

3. Towards more realistic screening

We noticed in the previous section that the macroscopic dielectric constant ε_∞ calculated in RPA with the PBE+U functional is significantly higher than the experimental value, despite the fact that the peak positions and relative intensities of the PBE+U loss function match well the available experimental data. In principle, an overestimated dielectric constant should go along with an underestimation of the band gap—the opposite of what we find. This observation may be interpreted as a hint that details of the dielectric function must be crucial for the screening mechanisms in CuO. For instance, short-range contributions to the screening might be particularly important for the localized d electrons.

It is, hence, not clear whether the failure of the GW formalism to predict the band gap of CuO is due to a deficient description of the screening function or whether higher-order terms, i.e., vertex corrections, have to be included in the self-energy. However, before resorting to more complicated theories demanding even more involved calculations, it would be desirable to obtain state-of-the-art experimental data for the

TABLE III. Local magnetic moments μ at the Cu and O atoms calculated for flavors of the GW approximation where the QP wave functions change with respect to the HSE06 and PBE+U ($U = 4$ eV) starting electronic structures. Furthermore, the magnetic moments in the self-consistent COHSEX approximation are given.

μ (μ_B)		DFT	scG_nW_0	scG_nW_n
HSE06	Cu	0.66	0.69	0.70
	O	0.13	0.12	0.12
PBE+U	Cu	0.55	0.64	0.70
	O	0.14	0.13	0.12
COHSEX	Cu			0.67
	O			0.12

wave-vector- and frequency-dependent dielectric function in a wide spectral range in order to have a better comparison between theory and experiment. This will allow one to understand the mechanisms that reign the screening in CuO.

4. *Local magnetic moments*

In Table III, the local magnetic moments at the Cu and O atoms are listed for the DFT starting electronic structures and those flavors of the GW approximation which allow for a change in the wave functions and, concomitantly, the local magnetic moments. While the magnetic moments of the O atoms are almost independent of the approach, the local moments at the Cu atoms increase with increasing band gap. We attribute this to a stronger separation between the spin-up and spin-down channels of the Cu $3d_{x^2-y^2}$ orbital with increasing band gap [see also Fig. 6(b)]. However, all of the GW results are within the error bars of the experimentally determined magnetic moments which amount to $0.65 \pm 0.03\mu_B$ [9] and $0.69 \pm 0.05\mu_B$ [10].

V. COMPARISON TO PHOTOEMISSION SPECTRA

The band gap is just one characteristic of the electronic excitation spectrum of an insulator which contains too little information to draw conclusions about the electronic structure as a whole. Thus, we now focus on the comparison between the calculated QP DOS and available photoemission spectra. In Fig. 9(a), the QP electronic structures obtained within the HSE06+sc$G_nW_0^{\mathrm{HSE06}}$, PBE+U+sc$G_nW_0^{\mathrm{PBE}+U}$, and scG_nW_n schemes are compared to x-ray photoemission spectroscopy [4,16] (XPS) and bremsstrahlung-isochromat spectroscopy [4] (BIS) data. To this end, we go beyond the assumption of a noninteracting shape for the QP Green's function and introduce instead the renormalized QP Green's function

$$G(\omega) = \sum_i Z_i \frac{|\psi_i\rangle\langle\psi_i|}{\hbar\omega - \varepsilon_i - i\hbar/\tau_i \,\mathrm{sgn}(\mu - \varepsilon_i)} \tag{5}$$

that is weighted by the QP renormalization factor Z_i and contains the intrinsic widths of the QP peaks, which are the inverses of the QP lifetimes

$$\tau_i = \frac{\hbar}{Z_i |\langle\psi_i| \,\mathrm{Im}\,\Sigma_{GW}(\varepsilon_i)|\psi_i\rangle|}. \tag{6}$$

The chemical potential is denoted by μ. In this approximation, the peak widths are given by the product of the QP renormalization factor Z_i and the imaginary part of the self-energy at the QP excitation. Consequently, the sum over δ functions in the QP DOS is replaced by a sum over non-normalized Lorentzians with widths corresponding to the intrinsic QP lifetime of each excitation,

$$\mathrm{DOS}(\hbar\omega) = \sum_i \frac{Z_i}{\pi} \frac{\hbar/\tau_i}{(\hbar\omega - \varepsilon_i)^2 + (\hbar/\tau_i)^2}. \tag{7}$$

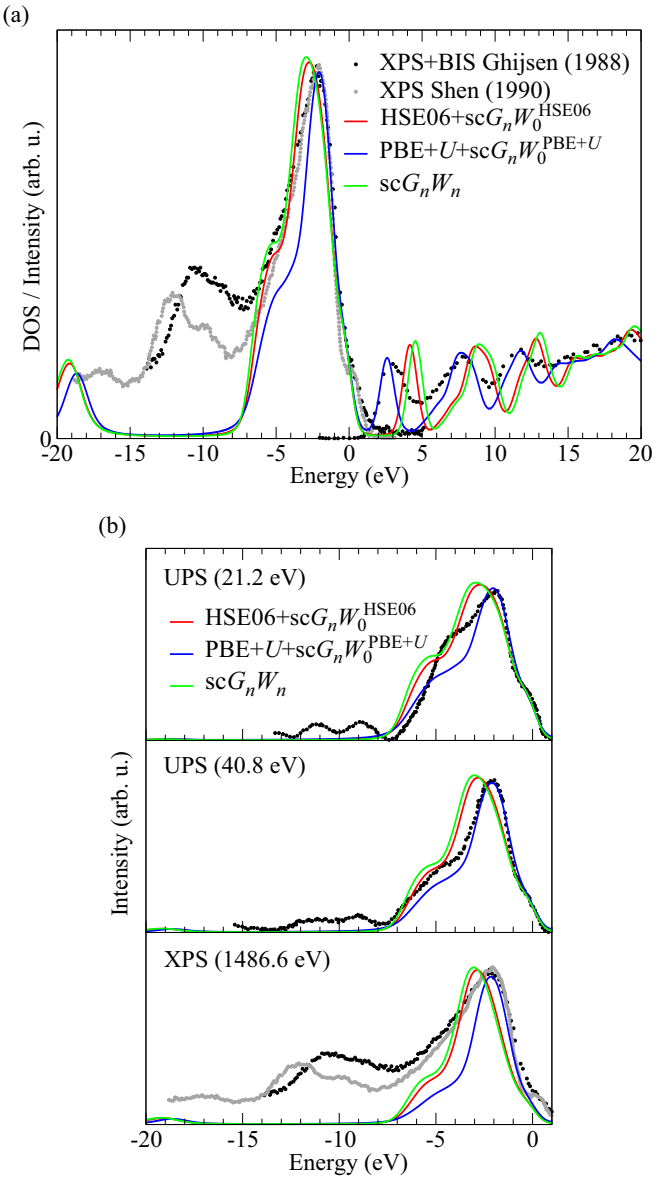

FIG. 9. (Color online) QP DOS of CuO compared to data from UPS, XPS, and BIS experiments. (a) QP DOS including intrinsic QP lifetimes are plotted together with XPS [4,16] (taken at an incident photon energy of 1486.6 eV) and BIS [4] data. A Gaussian broadening of 1.0 eV (FWHM) is applied to the calculated spectra to mimic temperature and instrumental broadening effects. In (b), the QP DOS are additionally weighted with the photoionization cross sections [74] of each orbital to facilitate comparison with photoemission spectra for various incident photon energies. Experimental data from Ghijsen *et al.* [4] and Shen *et al.* [16] are shown as black and gray dots.

TABLE IV. QP renormalization factors Z for the highest valence (Γ_{VBM}) and lowest conduction band (Γ_{CBM}) at Γ calculated in various flavors of the GW approximation starting from HSE06 and PBE+U ($U = 4$ eV) electronic structures.

Z		G_0W_0	G_nW_0	G_nW_n	scG_nW_0	scG_nW_n
HSE06	Γ_{VBM}	0.74	0.73	0.74	0.73	0.76
	Γ_{CBM}	0.71	0.70	0.72	0.70	0.73
PBE+U	Γ_{VBM}	0.65	0.64	0.69	0.64	0.75
	Γ_{CBM}	0.62	0.62	0.67	0.60	0.73

Further, the DOS are convoluted with a Gaussian of 1.0 eV (FWHM) to take into account instrumental and temperature broadening effects.

In Table IV, the QP renormalization factors are given for the highest valence and lowest conduction band at the Γ point. The Z factors essentially follow the trend of the band gaps in the electronic structure used to calculate the screened Coulomb interaction. A high band gap in W shifts the onset of the imaginary part of the self-energy away from the QP poles, thus resulting in a more pronounced QP peak. Consequently, the QP renormalization factors are closest to one for the scG_nW_n scheme and depend strongly on the W employed, whereas they are basically insusceptible to self-consistency in G. A comparison between Figs. 6(a) and 9(a) shows that in particular the valence Cu 3d peak which is more pronounced in the PBE+U+sc$G_nW_0^{\mathrm{PBE}+U}$ approach is reduced to the same intensity as the equivalent peak in the HSE06+sc$G_nW_0^{\mathrm{HSE06}}$ or scG_nW_n approaches due to the smaller Z factors in the former GW scheme.

Comparing theory and experiment in Fig. 9(a), we find very good agreement for the peak positions, widths, and relative intensities in the range of QP valence excitations between -8 and 0 eV. Differences between the theoretical approaches in the valence-band region are too small to rule out one or more of the theoretical schemes. However, the PBE+U+sc$G_nW_0^{\mathrm{PBE}+U}$ approach seems to perform slightly better concerning the general line shape. The satellite structures that occur in the vicinity of -10 eV can, by definition, not be captured in our QP framework. The O 2s states around -19 eV are strongly broadened by lifetime effects.

The conduction-band region is dominated by a distinct peak at low energies that stems from the empty Cu $3d_{x^2-y^2}$ band in the minority spin channel. All three theoretical approaches agree very well with the experimental BIS data regarding peak widths and relative intensities. Only the band gap differs significantly (see discussion in Sec. IV). The PBE+U+sc$G_nW_0^{\mathrm{PBE}+U}$ iteration scheme actually yields also peak positions that match the experimental inverse-photoemission peaks. Notably, the edge of the first conduction-band peak agrees well with the first BIS peak, even though the gap of 1.4 ± 0.3 eV deduced from experiment in Ref. [4] deviates from our gap value of 2.2 eV. It cannot be excluded that, apart from temperature effects, also different procedures to determine the gap are, to some extent, responsible for the discrepancy.

Photoemission spectra for CuO have been measured at various incident photon energies [see Fig. 9(b)]. This allows us to extract information about the orbital character of the valence states, since the photoionization cross sections of different orbitals vary with the incident photon energy. At high photon energies, primarily d states are probed, whereas at lower photon energies, in the UV, p and d states are excited with roughly the same probabilities. In Fig. 9(b), the calculated QP DOS weighted by photoionization cross sections [74] are compared to photoemission data taken at different energies. With increasing photon energy, the shoulders found around -5 eV and near the VBM in the experimental data decrease in intensity relative to the main photoemission peak. This behavior is due to the O 2p orbital contribution to these peaks [mixed with Cu $3d_{x^2-y^2}$ states; see Fig. 6(b)] which is suppressed at higher incident energies. Despite the intense background in the experimental data for 1486.6 eV incident photon energy, also the strongly damped O 2s peak is visible. As in the case of the loss function, details of the photoemission spectra are thus very well described besides a constant shift of the conduction states that stems from the band-gap problem.

VI. SUMMARY AND CONCLUSIONS

We performed state-of-the-art many-body calculations in the GW approximation to compute the electronic QP excitation spectrum of the strongly correlated oxide CuO. In a first step, DFT was used to calculate starting electronic structures using the HSE06 and PBE+U exchange-correlation functionals. These functionals already account for large parts of the static screened exchange on the open Cu 3d shell and yield—apart from the band gap—almost identical DOS.

Subsequently, the performance of various recently proposed GW self-consistency schemes has been investigated. Aside from the general line shape of the QP DOS, the comparison focuses on the band gap as a characteristic quantity of each insulator. We find the band gap of CuO to be extremely sensitive to the details of the GW iteration scheme. Non-self-consistent and eigenvalue-self-consistent GW schemes are strongly starting-point dependent, since they do not update the one-particle wave functions. QP self-consistent GW, on the other hand, which updates also the wave functions, overestimates the band gap of CuO dramatically, since it removes the error cancellation between neglected QP effects and neglected excitonic effects in the dielectric screening by including only QP corrections in the self-consistency cycle.

That is why we resort to a QP self-consistent GW scheme where the screened Coulomb interaction compares well to the inverse dielectric function found in loss experiments and is kept fixed during the iteration. We find that the fundamental gap is still, albeit much less, overestimated within this approach. Our results indicate that the clue to the understanding of the electronic structure of CuO, and in particular the band gap, lies in the details of the screening. Therefore, momentum- and frequency-resolved experimental data for the dielectric function of CuO are urgently needed.

Apart from the gap, excellent agreement of the calculated QP spectra with the QP excitations in direct and inverse photoemission experiments is found, in particular when intrinsic QP lifetimes and matrix-element effects are taken into account.

ACKNOWLEDGMENTS

We are grateful for valuable discussions with G. Kresse, S. Huotari, P. Schattschneider, F. Bechstedt, M. Gatti, and X. Rocquefelte. Financial support has been provided by the European Commission Marie Curie Actions within the framework of the CEA Eurotalents program and the European Research Council under the European Union's 7th Framework Program (ERC Grant Agreement No. 320971). This work has benefited from collaboration with the Maison de la Simulation. Computer time has been provided by GENCI (Project No. 544).

[1] M. Heck and P. Hoffmann, Archaeometry **42**, 341 (2000).
[2] B. K. Meyer, A. Polity, D. Reppin, M. Becker, P. Hering, P. J. Klar, T. Sander, C. Reindl, J. Benz, M. Eickhoff, C. Heiliger, M. Heinemann, J. Bläsing, A. Krost, S. Shokovets, C. Müller, and C. Ronning, Phys. Status Solidi B **249**, 1487 (2012).
[3] F. P. Koffyberg and F. A. Benko, J. Appl. Phys. **53**, 1173 (1982).
[4] J. Ghijsen, L. H. Tjeng, J. van Elp, H. Eskes, J. Westerink, G. A. Sawatzky, and M. T. Czyzyk, Phys. Rev. B **38**, 11322 (1988).
[5] J. G. Bednorz and K. A. Müller, Z. Phys. B **64**, 189 (1986).
[6] A. J. Leggett, Nat. Phys. **2**, 134 (2006).
[7] T. Kimura, Y. Sekio, H. Nakamura, T. Siegrist, and A. P. Ramirez, Nat. Mater. **7**, 291 (2008).
[8] S. Åsbrink and L.-J. Norrby, Acta Crystallogr. B **26**, 8 (1970).
[9] J. B. Forsyth, P. J. Brown, and B. M. Wanklyn, J. Phys. C **21**, 2917 (1988).
[10] B. X. Yang, T. R. Thurston, J. M. Tranquada, and G. Shirane, Phys. Rev. B **39**, 4343 (1989).
[11] W. Y. Ching, Y.-N. Xu, and K. W. Wong, Phys. Rev. B **40**, 7684 (1989).
[12] F. Marabelli, G. B. Parravicini, and F. Salghetti-Drioli, Phys. Rev. B **52**, 1433 (1995).
[13] A. Svane and O. Gunnarsson, Phys. Rev. Lett. **65**, 1148 (1990).
[14] Z. Szotek, W. M. Temmerman, and H. Winter, Phys. Rev. B **47**, 4029 (1993).
[15] A. Filippetti and V. Fiorentini, Phys. Rev. Lett. **95**, 086405 (2005).
[16] Z.-X. Shen, R. S. List, D. S. Dessau, F. Parmigiani, A. J. Arko, R. Bartlett, B. O. Wells, I. Lindau, and W. E. Spicer, Phys. Rev. B **42**, 8081 (1990).
[17] L. Hedin, Phys. Rev. **139**, A796 (1965).
[18] L. Hedin and S. Lundqvist, in *Solid State Physics. Advances in Research and Applications*, edited by F. Seitz, D. Turnbull, and H. Ehrenreich (Academic Press, New York, 1969), Vol. 23, p. 1.
[19] W. G. Aulbur, L. Jönsson, and J. W. Wilkins, *Solid State Physics. Advances in Research and Applications*, edited by H. Ehrenreich and F. Spaepen (Academic Press, San Diego, 1999), Vol. 54, p. 1.
[20] S. V. Faleev, M. van Schilfgaarde, and T. Kotani, Phys. Rev. Lett. **93**, 126406 (2004).
[21] F. Bruneval, N. Vast, and L. Reining, Phys. Rev. B **74**, 045102 (2006).
[22] M. Gatti, F. Bruneval, V. Olevano, and L. Reining, Phys. Rev. Lett. **99**, 266402 (2007).
[23] C. Rödl, F. Fuchs, J. Furthmüller, and F. Bechstedt, Phys. Rev. B **79**, 235114 (2009).
[24] H. Jiang, R. I. Gomez-Abal, P. Rinke, and M. Scheffler, Phys. Rev. B **82**, 045108 (2010).
[25] M. S. Hybertsen and S. G. Louie, Phys. Rev. B **34**, 5390 (1986).
[26] J. Heyd, G. E. Scuseria, and M. Ernzerhof, J. Chem. Phys. **118**, 8207 (2003).
[27] V. I. Anisimov, J. Zaanen, and O. K. Andersen, Phys. Rev. B **44**, 943 (1991).
[28] S. L. Dudarev, G. A. Botton, S. Y. Savrasov, C. J. Humphreys, and A. P. Sutton, Phys. Rev. B **57**, 1505 (1998).
[29] D. Wu, Q. Zhang, and M. Tao, Phys. Rev. B **73**, 235206 (2006).
[30] M. Heinemann, B. Eifert, and C. Heiliger, Phys. Rev. B **87**, 115111 (2013).
[31] X. Rocquefelte, M.-H. Whangbo, A. Villesuzanne, S. Jobic, F. Tran, K. Schwarz, and P. Blaha, J. Phys.: Condens. Matter **22**, 045502 (2010).
[32] S. Lany, Phys. Rev. B **87**, 085112 (2013).
[33] K. Momma and F. Izumi, J. Appl. Crystallogr. **44**, 1272 (2011).
[34] G. Kresse and J. Furthmüller, Comput. Mater. Sci. **6**, 15 (1996).
[35] G. Kresse and D. Joubert, Phys. Rev. B **59**, 1758 (1999).
[36] M. Shishkin and G. Kresse, Phys. Rev. B **74**, 035101 (2006).
[37] M. Shishkin and G. Kresse, Phys. Rev. B **75**, 235102 (2007).
[38] A. V. Krukau, O. A. Vydrov, A. F. Izmaylov, and G. E. Scuseria, J. Chem. Phys. **125**, 224106 (2006).
[39] J. P. Perdew, K. Burke, and M. Ernzerhof, Phys. Rev. Lett. **77**, 3865 (1996).
[40] V. Olevano, L. Reining, and F. Sottile, http://dp-code.org.
[41] M. Shishkin, M. Marsman, and G. Kresse, Phys. Rev. Lett. **99**, 246403 (2007).
[42] W. Setyawan and S. Curtarolo, Comput. Mater. Sci. **49**, 299 (2010).
[43] B.-C. Shih, Y. Xue, P. Zhang, M. L. Cohen, and S. G. Louie, Phys. Rev. Lett. **105**, 146401 (2010).
[44] M. Stankovski, G. Antonius, D. Waroquiers, A. Miglio, H. Dixit, K. Sankaran, M. Giantomassi, X. Gonze, M. Côté, and G.-M. Rignanese, Phys. Rev. B **84**, 241201 (2011).
[45] C. Friedrich, M. C. Müller, and S. Blügel, Phys. Rev. B **83**, 081101 (2011).
[46] J. Klimeš, M. Kaltak, and G. Kresse, Phys. Rev. B **90**, 075125 (2014).
[47] J. P. Perdew and M. Levy, Phys. Rev. Lett. **51**, 1884 (1983).
[48] L. J. Sham and M. Schlüter, Phys. Rev. Lett. **51**, 1888 (1983).
[49] A. Seidl, A. Görling, P. Vogl, J. A. Majewski, and M. Levy, Phys. Rev. B **53**, 3764 (1996).
[50] J. P. Perdew, Adv. Quantum Chem. **21**, 113 (1990).
[51] M. Cococcioni and S. de Gironcoli, Phys. Rev. B **71**, 035105 (2005).
[52] F. Aryasetiawan, M. Imada, A. Georges, G. Kotliar, S. Biermann, and A. I. Lichtenstein, Phys. Rev. B **70**, 195104 (2004).
[53] M. van Schilfgaarde, T. Kotani, and S. Faleev, Phys. Rev. Lett. **96**, 226402 (2006).
[54] R. Sakuma, T. Miyake, and F. Aryasetiawan, Phys. Rev. B **80**, 235128 (2009).
[55] A. N. Chantis, M. van Schilfgaarde, and T. Kotani, Phys. Rev. B **76**, 165126 (2007).

[56] J. Heyd, J. E. Peralta, G. E. Scuseria, and R. L. Martin, J. Chem. Phys. **123**, 174101 (2005).
[57] F. Fuchs, J. Furthmüller, F. Bechstedt, M. Shishkin, and G. Kresse, Phys. Rev. B **76**, 115109 (2007).
[58] M. A. L. Marques, J. Vidal, M. J. T. Oliveira, L. Reining, and S. Botti, Phys. Rev. B **83**, 035119 (2011).
[59] K. V. Rao and A. Smakula, J. Appl. Phys. **37**, 2840 (1966).
[60] G. Kliche and Z. V. Popovic, Phys. Rev. B **42**, 10060 (1990).
[61] T. Ito, H. Yamaguchi, T. Masumi, and S. Adachi, J. Phys. Soc. Jpn. **67**, 3304 (1998).
[62] A. B. Kuz'menko, D. van der Marel, P. J. M. van Bentum, E. A. Tishchenko, C. Presura, and A. A. Bush, Phys. Rev. B **63**, 094303 (2001).
[63] T. Masumi, H. Yamaguchi, T. Ito, and H. Shimoyama, J. Phys. Soc. Jpn. **67**, 67 (1998).
[64] C. Rödl, F. Fuchs, J. Furthmüller, and F. Bechstedt, Phys. Rev. B **77**, 184408 (2008).
[65] P. Liao and E. A. Carter, Phys. Chem. Chem. Phys. **13**, 15189 (2011).
[66] W. B. Wu, N. Hiraoka, D. J. Huang, S. W. Huang, K. D. Tsuei, M. van Veenendaal, J. van den Brink, Y. Sekio, and T. Kimura, Phys. Rev. B **88**, 205129 (2013).
[67] S. Huotari, L. Simonelli, C. J. Sahle, M. Moretti Sala, R. Verbeni, and G. Monaco, J. Phys.: Condens. Matter **26**, 165501 (2014).
[68] E. A. Bakulin, M. M. Bredov, E. G. Ostroumova, and V. V. Shcherbinina, Fiz. Tverd. Tela (Leningrad) **19**, 1307 (1977) [Sov. Phys. Solid State **19**, 760 (1977)].
[69] N. Vast, L. Reining, V. Olevano, P. Schattschneider, and B. Jouffrey, Phys. Rev. Lett. **88**, 037601 (2002).
[70] S. Botti and M. A. L. Marques, Phys. Rev. Lett. **110**, 226404 (2013).
[71] G. D. Mahan, *Many-Particle Physics*, 2nd ed. (Plenum Press, New York, 1990).
[72] F. Bechstedt, K. Seino, P. H. Hahn, and W. G. Schmidt, Phys. Rev. B **72**, 245114 (2005).
[73] *Springer Handbook of Condensed Matter and Materials Data*, edited by W. Martienssen and H. Warlimont (Springer, Berlin, 2005).
[74] J. J. Yeh and I. Lindau, At. Data Nucl. Data Tables **32**, 1 (1985).